analytical chemistry

pubs.acs.org/ac

Article

Structural and Functional Characterization of SARS-CoV-2 RBD Domains Produced in Mammalian Cells

Christoph Gstöttner, Tao Zhang, Anja Resemann, Sophia Ruben, Stuart Pengelley, Detlev Suckau, Tim Welsink, Manfred Wuhrer, and Elena Domínguez-Vega*

Cite This: *Anal. Chem.* 2021, 93, 6839−6847

Read Online

ACCESS | Metrics & More | Article Recommendations | Supporting Information

ABSTRACT: As the severe acute respiratory syndrome coronavirus 2 (SARS-CoV-2) pandemic is still ongoing and dramatically influences our life, the need for recombinant viral proteins for diagnostics, vaccine development, and research is very high. The spike (S) protein, and particularly its receptor-binding domain (RBD), mediates the interaction with the angiotensin-converting enzyme 2 (ACE2) receptor on host cells and may be modulated by its structural features. Therefore, well-characterized recombinant RBDs are essential. We have performed an in-depth structural and functional characterization of RBDs expressed in Chinese hamster ovary (CHO) and human embryonic kidney 293 (HEK293) cells. To structurally characterize the native RBDs (comprising *N*- and *O*-glycans and additional post translational modifications), a multilevel mass spectrometric approach was employed. Released glycan and glycopeptide analysis were integrated with intact mass analysis, glycan-enzymatic dissection, and top-down sequencing for comprehensive annotation of RBD proteoforms. The data showed distinct glycosylation for CHO- and HEK293-RBD with the latter exhibiting antenna fucosylation, a higher level of sialylation, and a combination of core 1 and core 2 type *O*-glycans. Additionally, using an alternative approach based on N-terminal cleavage of the O-glycosylation, the previously unknown O-glycosylation site was localized at T323. For both RBDs, the binding to SARS-CoV-2 antibodies of positive patients and affinity to the ACE2 receptor was addressed showing comparable results. This work not only offers insights into RBD structural and functional features but also provides an analytical workflow for characterization of new RBDs and batch-to-batch comparison.

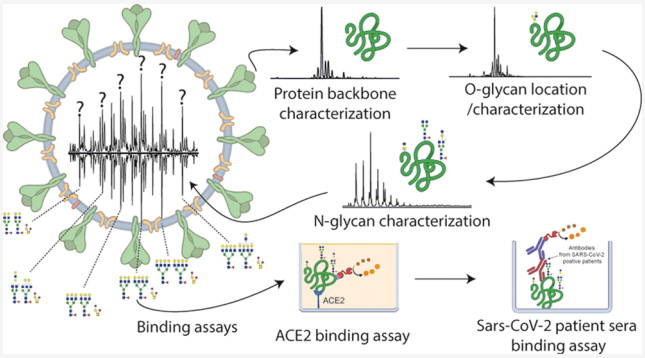

Since the outbreak of coronavirus disease 2019 (COVID-19), the severe acute respiratory syndrome coronavirus 2 (SARS-CoV-2) virus has infected more than 100 million individuals and influences our daily lives. The coronavirus is an enveloped RNA virus containing three different structural proteins in the membrane, the envelop (E) protein, the membrane (M) protein, and the spike (S) glycoprotein.[1] The S protein is heavily glycosylated and forms a trimer on the SARS-CoV-2 surface. Each S protein carries 22 N-glycosylation sites[2] and consists of S1 and S2 subunits. Whereas the S2 subunit is necessary for membrane fusion, the S1 subunit directly interacts with the angiotensin-converting enzyme 2 (ACE2) receptor in the human respiratory tract and facilitates the entry into the host cell.[3] In particular, the receptor-binding domain (RBD) of the S1 subunit mediates the interaction with the ACE2 receptor.[4] This domain carries two N-linked glycans at positions N331 and N343 and, depending on the source, one or two O-linked glycosylation sites (T323/S325) are occupied.[2,5,6] The predicted *O*-glycosylation site at T323 is not present in the S protein of SARS-CoV-1 and has been hypothesized to have an influence on the interaction with the ACE2 receptor[7] and may be critical for conformational changes of the RBD.[8] Further studies have shown the role of glycosylation on ACE2−RBD binding. Crystallographic structures have confirmed the interaction between RBD and the ACE2 receptor and highlighted the importance of ACE2 glycosylation in the interaction.[9] However, the RBD used was expressed in insect cells, and the role of RBD glycosylation was not addressed.[9] In a more recent publication, the interaction of the *N*-glycan at position N343 of the RBD with the ACE2 receptor has been suggested by modeling the interaction using atomistic molecular dynamic simulations.[10] Another study revealed that the infectivity decreased by 1200 times (decrease of relative infectivity to 0.083%) when both N-glycosylation sites (N331 and N343) of the spike protein were silenced compared to the wild-type versions. These findings suggest

Received: February 27, 2021
Accepted: April 9, 2021
Published: April 19, 2021

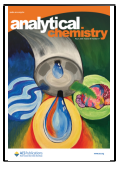

https://doi.org/10.1021/acs.analchem.1c00893
Anal. Chem. 2021, 93, 6839−6847

that glycosylation is involved in the binding to the receptor, either directly or by providing conformational stabilization.[11] In line with its role in virus−ACE2 interaction, the RBD is the primary target of neutralizing antibodies.[12] Interestingly, an antibody named S309, pulled from serum from a SARS-CoV-1 recovered patient, bound an epitope containing also glycosylation.[13] This binding site is also conserved in SARS-CoV-2 and was predicted as an epitope for neutralizing antibodies.[14] The neutralizing S309 antibody was shown to bind to a protein epitope (331−344) in combination with the glycan at N343. The antibody showed especially strong interaction with the core fucose and to a minor extent with the remaining glycan structure.[13] All of these findings emphasize that the assessment of RBD glycosylation is highly important.

Recombinantly produced S proteins are essential tools in the fight against SARS-CoV-2, contributing to a further understanding of the interaction mechanism, providing efficient components for diagnostic purposes and helping in vaccine development.[15] However, it is important to understand that glycosylation and other structural characteristics may differ considerably between different biotechnologically produced proteins and their natural forms. Considering the relevance of RBD glycosylation on ACE2 binding and recognition by neutralizing antibodies, the use of well-characterized S proteins is essential. The S protein, in particular, has been produced as a full-length protein as well as in a short version containing the RBD.[16] Site-specific glycosylation analysis of the 22 N-glycosylation sites of the recombinant S glycoprotein expressed in human embryonic kidney 293 (HEK293) cells showed mainly complex type glycans but also, at certain glycosylation sites, high mannose structures and in lower amounts, some hybrid structures.[2,5] In particular, the two N-glycosylation sites (N331 and N343), which are located in the RBD were found to carry mainly complex type glycans as well as spurious amounts of high mannose glycans. Similarly, for the S1 subunit recombinantly produced in HEK293 cells, mainly complex type glycans were found at both sites.[5] As predicted by Uslupehlivan and Şener,[7] O-glycosylation at the position T323 and/or at S325 was found. Whereas one report, analyzing the whole S protein recombinantly produced, showed only trace levels of *O*-glycans,[2] another study detected high levels of O-glycosylation.[6] Still, in these studies, the localization of the O-glycosylation site at T323 and/or S325 was not possible. O-glycosylation at these two positions is also thought to be important to stabilize the conformation of the RBD or to introduce conformational changes.[8] All of these studies have been performed using recombinant versions of the spike protein or subunits thereof. Interestingly, upon expression in HEK293 cells, the amount of sialic acids varied from low to high depending on whether the complete S protein or only the S1 subunit was produced,[5] suggesting that the N- and O-glycosylation is dependent on the context of the protein (S, S1, or RBD only). So far, only terminal glycan epitopes of HEK293-produced RBD have been studied by NMR; however, an assessment of the entire *N*-glycan structure, composition, and the relative quantification of the *N*-glycans could not be achieved.[17] Furthermore, the O-glycosylation was neglected completely. Also, a characterization of the intact RBD is still missing, providing information on the combination of the glycans as well as on additional protein backbone modifications.

Here, we present an in-depth structural and functional characterization of two commercially available SARS-CoV-2 RBDs produced in two different expression systems, HEK293 and Chinese hamster ovary (CHO) cells. To achieve comprehensive structural information, a multilevel characterization was performed (Figure 1). Both RBD samples were

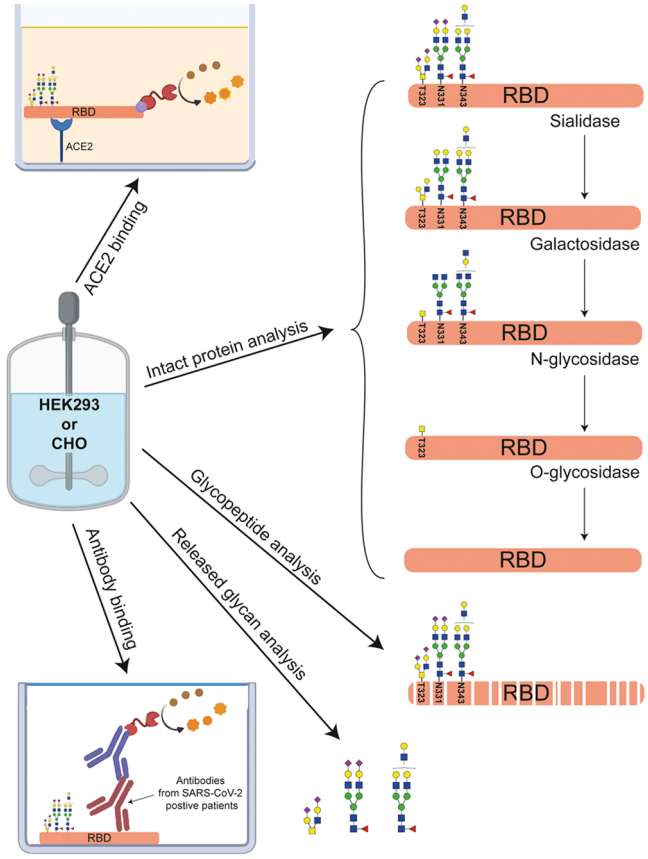

Figure 1. Multilevel characterization of CHO- and HEK293-RBD. Next to intact protein analysis using CE-MS and MALDI-ISD-MS, the samples are structurally characterized by glycan dissection, glycopeptide analysis, and released glycan analysis. Their functional characterization was performed by measuring their binding characteristics to ACE2 and anti-SARS-CoV-2 antibodies.

initially analyzed at the intact level by top-down sequencing using matrix-assisted laser desorption ionization (MALDI) in-source-decay (MALDI-ISD) mass spectrometry (MS)[18,19] and by sheathless capillary electrophoresis (CE)-MS after full N- and O-deglycosylation to establish their protein sequences and putative nonglycan modifications. With the established sequences and the help of sequential glycosidase treatment, the glycoforms on both N- and the O-glycosylation sites were assigned. Our findings were confirmed by glycopeptide analysis and the analysis of released *O*-glycans by porous graphitized carbon (PGC) nanoliquid chromatography electrospray ionization tandem mass spectrometry (LC-ESI-MS/MS). To assess functional differences between the two RBD samples, we determined their binding characteristics to ACE2 and sera of patients who recovered from a previous SARS-CoV-2 infection.

EXPERIMENTAL SECTION

Reagents and Samples. Reagents used for this study were at least of analytical grade; for more details, see Supporting Information S1. Recombinant RBDs (Wuhan-Hu-1-isolate

https://doi.org/10.1021/acs.analchem.1c00893
Anal. Chem. 2021, 93, 6839−6847

(MN908947)), either transiently expressed in HEK293 or stably expressed in CHO cells, were used (InVivo Biotech Services, Henningsdorf, Germany). The constructs contained the amino-acid sequence 319 to 541 with a C-terminal 6xHis-Tag. Recombinant RBDs were purified using immobilized metal affinity chromatography and a size-exclusion polishing step. The samples were stored in 20 mM sodium phosphate, 300 mM NaCl, pH 7.2. Glycosidases SialEXO (sialidases α2-3, α2-6, and α2-8), GalactEXO (galactosidases β1-3 and β1-4), OglyZOR (endo-α-*N*-acetylgalactosaminidase), OpeRATOR (*O*-protease), α1-2 fucosidase, and α1-3,4 fucosidase were obtained from Genovis (Lund, Sweden). Peptide *N*-glycosidase F (PNGaseF) was purchased from Roche Diagnostics (Mannheim, Germany).

Intact RBD Analysis by Sheathless CE-MS. Samples for intact protein analysis were buffer exchanged with Tris pH 6.8 using 10 kDa Vivaspin MWCO filters Sartorius (Göttingen, Germany) to a final concentration of 1 μg/μL. Subsequently the enzymes SialEXO, GalactEXO, OglyZOR, or OpeRATOR were added according to the producer specifications and incubated overnight at 37 °C. PNGaseF was added in a ratio of 1:5 (v/v) and incubated overnight at 37 °C. For removing antenna fucosylation, 20 μg of the HEK293-RBD sample was incubated with 4.4 μg of fucosidase α1-2 or 8.8 μg of fucosidase α1-3,4 overnight at 37 °C. Afterward, all samples were buffer exchanged with 100 mM ammonium acetate, pH 3.0, and subsequently analyzed by sheathless CE-MS. For sheathless CE measurements, a Sciex CESI 8000 instrument combined with a Bruker Impact qTOF-MS was used. Bare-fused silica CE capillaries were obtained from Sciex (Framingham, MA) and subsequently coated with polyethylenimine (PEI).[20] Afterward, the sample was injected (15 s, 5 psi) and analyzed by applying 20 kV (reversed polarity) at 20 °C for 45 min. For detailed CE and MS settings, see Supporting Information S2. Intact RBD data were deconvoluted using DataAnalysis 5.3 (Bruker Daltonics) maximum entropy algorithm. Deconvoluted mass spectra were baseline subtracted and smoothed using the Gaussian smoothing function with a width of 0.5 Da and one cycle. Glycoforms were assigned based on the average masses observed and observed mass shifts with enzyme treatments. Reconstructed intact spectra from bottom-up data were simulated using an algorithm in R developed by Yang et al., which is publicly available and can be found at https://github.com/Yang0014/glycoNativeMS.[21] For our data, instead of simulating the charge-state distribution of the protein, we simulated the deconvoluted mass spectra so no correction for the relative abundance of different charge states needed to be performed.

MALDI-ISD Top-Down Protein Sequence Analysis. Fully deglycosylated RBD samples were reduced for 30 min at 50 °C using dithiothreitol (DTT). Two microliters of the reduced sample was spotted on a hydrophilic anchor of an MTP BigAnchor sample plate and incubated. After 2 min, the remaining droplet was removed and the spot was washed using 0.1% trifluoroacetyl (TFA) in water. Subsequently, 1 μL of a super-DHB (sDHB) matrix solution (25 μg/μL in 50% acetonitrile/49.9% water/0.1% TFA) was deposited on the dried sample spot. MALDI-ISD spectra were acquired with a rapifleX MALDI-TOF MS instrument (Bruker). Detailed MS settings and spectra assignment can be found in Supporting Information S3.

Glycopeptide Analysis by Reverse-Phase Liquid Chromatography (RPLC)-MS/MS. For glycopeptide generation, double digestion with trypsin followed by elastase was performed. In short, samples were reduced (45 mM DTT), alkylated (100 mM iodoacetamide (IAA)), and the reaction was stopped (45 mM DTT). After overnight tryptic digestion, the reaction was stopped (90 °C) and elastase was added. After overnight incubation with elastase, the reaction was stopped (formic acid). A more detailed description can be found in Supporting Information S4. The digested samples were separated using a nanoElute (Bruker) nanoflow ultrahigh-performance liquid chromatography (UHPLC) equipped with an Aurora 25 cm × 75 μm C18 column with a particle size of 1.6 μm (IonOpticks, Parkville, Victoria, Canada) and analyzed on a timsTOF PRO (Bruker). Information about the LC and MS parameters can be found in Supporting Information S5. MS/MS data of N-linked glycopeptides were generated following Hinneburg et al.[22] and processed using DataAnalysis 5.3 and MGF peak lists were imported into a BioPharma Compass 2021 (Bruker) and further analyzed using the glycopeptide analysis workflow. This workflow includes MS/MS spectra classification using typical fragmentation patterns to determine the peptide mass and the glycan mass. The peptide sequences were then identified using the theoretical digest feature of the software. In a second search, the classified MS/MS spectra were analyzed using the GlycoQuest search engine within BioPharma Compass 2021 software. For quantification, the most intense isotope of each charge state ($[M + H]^+$, $[M + 2H]^{2+}$, or $[M + 3H]^{3+}$) was extracted and the results normalized to the total peak intensity of all glycopeptides within one sample to 100%.

Released *O*-Glycan Analysis by PGC Nano-LC-ESI-MS/MS. Released *O*-glycan alditols from RBD samples were prepared using a 96-well plate sample preparation method, as previously described.[23] In brief, after *N*-glycan removal (PNGaseF, 2 U, overnight incubation at 37 °C), the *O*-glycans were released via reductive β-elimination. The analysis of *O*-glycan alditols was performed on an Ultimate 3000 UHPLC system (Dionex/Thermo) equipped with an in-house-packed PGC trap column (5 μm Hypercarb, 320 μm x 30 mm) and an in-house-packed PGC nanocolumn (Grace Discovery Sciences, Columbia, MD) (3 μm Hypercarb 100 μm x 150 mm) coupled to an amaZon ETD speed ion trap (Bruker) following a method described previously.[23] More detailed information can be found in the Supporting Information (Section S6). Structures of detected glycans were confirmed by MS/MS in a negative mode.[24] Glycan structures were assigned on the basis of the known MS/MS fragmentation patterns in a negative-ion mode,[25−27] elution order, and general glycobiological knowledge, with help of Glycoworkbench[28] and Glycomod software.[29] Relative quantification of individual glycans was performed by normalizing the total peak area of all glycans within one sample to 100%.

SARS-CoV-2-IgG Enzyme-Linked Immunosorbent Assay (ELISA) with RBD Antigens. The antigens (intact or glycosidase-treated HEK293-RBD or CHO-RBD) were used to coat immunoassay plates at a concentration of 2 μg/mL. Subsequently, blocking was performed with blocking buffer containing 1% bovine serum albumin (BSA). Serum collected >10 weeks after the onset of first symptoms from 12 SARS-CoV-2 polymerase chain reaction (PCR)-positive tested donors was applied to the RBD-coated wells at a dilution of 1:101. As a negative control, a 1:101 diluted serum pool containing 10 sera taken from healthy individuals in the year 2012 was used. The wells were washed three times with 250

https://doi.org/10.1021/acs.analchem.1c00893
Anal. Chem. 2021, 93, 6839−6847

μL of phosphate-buffered saline (PBS) containing 0.1% Tween 20. Subsequently, bound IgG from sera was detected by anti-human IgG-horseradish peroxidase (HRP) and developed with tetramethylbenzidine. The reaction was stopped using sulfuric acid. The absorbance was measured at 450 nm using a microplate reader. To determine the linear correlation between the absorption values, the Pearson correlation was calculated using GraphPad Prism 9. Linear regression was employed for the visualization of the correlation. For this analysis, the negative control value was excluded.

ACE2 Receptor-Binding Assay. Intact and glycosidase-treated RBD, S1 subunit, and the S protein (InVivo Biotech) were biotinylated using 10 molar excess of NHS-LC-Biotin (Thermo Scientific). Immunoassay plates were coated with 2.5 μg/mL recombinant angiotensin-converting enzyme 2 (ACE2, Sigma-Aldrich). Subsequently, the assay plate wells were blocked using blocking buffer containing 1% BSA. Dilutions of the biotinylated antigens ranging from 1 to 0.001 μg/mL were applied to the ACE2-coated assay plate wells in duplicates. The wells were washed three times with 250 μL of PBS containing 0.1% Tween 20. Bound biotinylated antigens were detected using a streptavidin peroxidase conjugate (Roche) and developed with tetramethylbenzidine. The reaction was stopped using sulfuric acid. The absorbance was measured at 450 nm using a microplate reader. GraphPad Prism 9 was used to plot log(dose) response curves (variable slope, four parameters) and to compute nonlinear fits, which were utilized to calculate the half-maximal concentrations (EC_{50}).

RESULTS AND DISCUSSION

Structural Characterization of CHO- and HEK293-RBD. We characterized the RBD domains (amino acids 319-541 containing a C-terminal His-tag) produced in CHO and HEK293 cells. This domain contains two N-glycosylation sites at positions N331 and N343 as well as two potential O-glycosylation sites at T323 and S325. Analysis of the intact RBDs revealed a complex pattern of signals comprising different *N*- and *O*-glycans and additional protein backbone modifications (see the Assessment of RBD N-glycosylation section). Therefore, to unravel this heterogeneity and achieve comprehensive structural characterization, we used a multilevel approach (Figure 1). Next, to classical released glycan and glycopeptide approaches, we applied a step-by-step dissection of glycans at the intact level similar to the work of Wohlschlager et al. for the biopharmaceutical etanercept.[30]

Characterization of the Protein Backbone after *N*- and *O*-Glycan Removal. To get information on the integrity of the protein backbone, the RBD proteins were treated with PNGaseF to remove the *N*-glycans and with an endo-*α*-*N*-acetylgalactosaminidase in combination with a mix of sialidases to remove the *O*-glycans. After deglycosylation, the RBDs were analyzed by CE-MS for intact mass and MALDI-ISD MS for top-down sequencing. Analysis of the samples by CE-MS resulted in one main peak in the base peak electropherogram (BPE) corresponding to the RBD. For the RBD produced in CHO cells, the observed averaged mass (26033.9 Da) was 119.0 Da higher than the theoretical mass calculated solely based on the amino-acid sequence (25914.9 Da) (Figure 2A). As the RBD contains a free cysteine at position C538,[31] it was presumably cysteinylated (+119.1 Da). This modification is often observed for free light chains during antibody production using CHO cells.[32] After reducing the disulfide bonds with

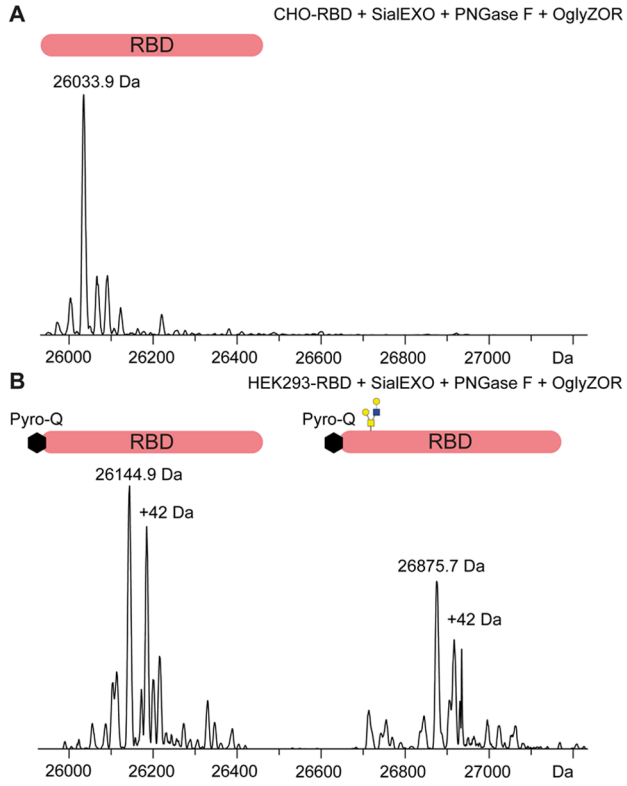

Figure 2. Deconvoluted ESI mass spectra of the main peak observed after sheathless CE-MS for (A) CHO-RBD and (B) HEK293-RBD. HEK293-RBD carries an additional N-terminal pyroglutamate. Blue square, *N*-acetylglucosamine; yellow square, *N*-acetylgalactosamine; and yellow circle, galactose.

DTT, the mass of the deglycosylated and completely reduced protein was 25923.0 Da, which is consistent with the expected theoretical mass (25923.0 Da), confirming the presence of cysteinylation (data not shown). For the RBD expressed in HEK293 cells, a deconvoluted mass of 26144.9 Da was observed (Figure 2B). Considering a cysteinylation of the free cysteine also in the HEK293-RBD, an additional mass difference of 110.9 Da was observed compared to the theoretical mass indicating additional modifications.

Both RBD samples were analyzed at the intact level by top-down sequencing using MALDI-ISD MS after full reduction and N- and O-deglycosylation. MALDI-ISD provides large terminal sequence tags and detects terminal (and internal) post translational modification (PTMs) from intact proteins. For both RBDs, we detected a C-terminal sequence tag of 73 amino acids (root-mean-square (RMS) error of 0.028 Da) verifying the expected C-terminus of the sequence. The N-terminal sequence tag, however, was not consistent between both RBDs. While the CHO-RBD sequence was in full agreement with the MALDI-ISD spectrum (Figure S1A), the HEK293-RBD sequence was found to be N-terminally extended by pyro-Glu (mass shift of 111.03 Da). Overall, 52% of the sequence was confirmed this way including an N-terminal sequence tag of 46 residues for the nonglycosylated and 29 residues for the O-glycosylated form (Figure S1B). Of note, the HEK293-RBD came with a slightly different sequence compared to the CHO-RBD, resulting in an additional glutamine at the N-terminus after cleavage of the signaling peptide (Figure S1B). Taking pyroglutamic acid formation into consideration, the measured mass perfectly fits the theoretical

https://doi.org/10.1021/acs.analchem.1c00893
Anal. Chem. 2021, 93, 6839−6847

mass (26145.1 Da). The N-terminal pyroglutamic acid formation was further confirmed by bottom-up analysis (data not shown). In addition, we found a species migrating before the main signal in the BPE with a +42.3 Da mass difference (26187.4 Da). This difference in mass might correspond to acetylation, however, it could not be confirmed by bottom-up analysis after trypsin digestion. This species was only observed in HEK293-RBD and not in CHO-RBD.

RBD *O*-Glycan Characterization. The RBD has two potential O-glycosylation sites at position T323 and S325. To characterize the *O*-glycans, the de-N-glycosylated RBDs (after treatment with PNGaseF) were analyzed by CE-MS (Figure S2) and the released *O*-glycans by PGC nano-LC-ESI-MS/MS (Figure 3), respectively. Table S1 summarizes the obtained

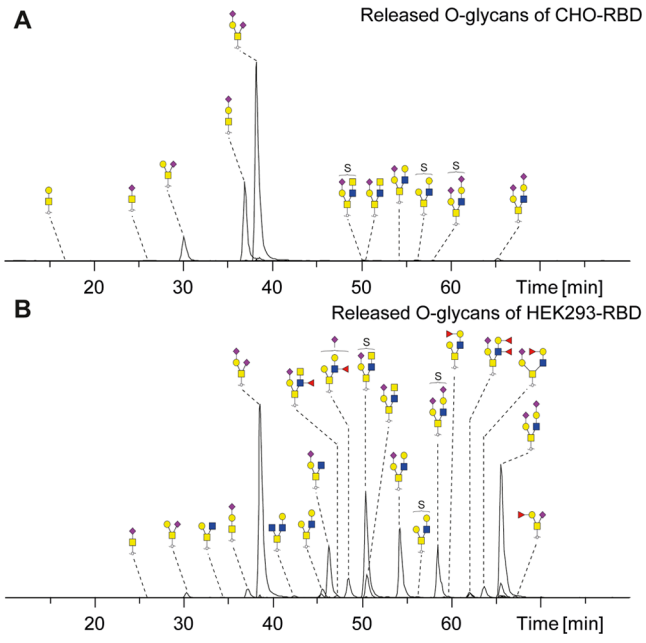

Figure 3. PGC nano-LC-ESI-MS/MS of released *O*-glycans from (A) CHO-RBD and (B) HEK293-RBD. Yellow square, *N*-acetylgalactosamine; yellow circle, galactose; blue square, *N*-acetylglucosamine; red triangle, fucose; purple diamond, *N*-acetylneuraminic acid (sialic acid); and S, sulfate.

results. In CHO-RBD, mainly core 1 structures with two sialic acids (H1N1S2) were observed. HEK293-RBD showed a much more diverse O-glycosylation pattern with a core 1 structure with two sialic acids as the main signal. Additionally, several core 2 structures, with and without fucose as well as with sulfation were detected. These data are in accordance with the data in Figure 2B for the sample treated with endo-*α*-*N*-acetylgalactosaminidase, where an additional signal of 26875.7 Da was observed. This mass corresponds to an H2N2 modification (theoretical mass 26875.8 Da), which is presumably a core 2 *O*-glycan, which cannot be cleaved by the endo-*α*-*N*-acetylgalactosaminidase. Similar glycoforms were not detected in CHO-RBD. The position of fucoses, either to the terminal galactose or the *N*-acetylglucosamine were confirmed by MS fragmentation and treatment with different fucosidases (Figure S3).

Hitherto published S protein bottom-up studies have not revealed the *O*-glycan attachment site, leaving both T323 and S325 as valid options.[2,6] To resolve this, we follow a different strategy based on *N*-glycan removal (with PNGaseF) and *O*-protease cleavage using the enzyme OpeRATOR in combination with a mix of sialidases. The *O*-protease cleaves the protein at the N-terminal site of an O-glycosylation site (Figure S3). This would result in a loss of the amino acids 319−322 from the RBD if the O-glycosylation is on T323 or 319−324 in case S325 carries *O*-glycan. As shown in Figure S4A, only one signal with a mass of 25919.0 Da was observed for the CHO material, which correlates to the RBD cleaved at T323 with a core 1 *O*-glycan H1N1 (theoretical mass 25918.8 Da). No RBD cleaved at S325 was observed. In HEK293-RBD, the same signal with a core 1 glycan H1N1 was observed also indicating that the glycosylation is located at T323 (Figure S4B). Next to this signal, an amount of uncleaved RBD with presumably core 2 *O*-glycan structures was detected. This is in line with a recent article that shows that the used *O*-protease can cleave N-terminal to core 1 but not core 2 glycan structures, similar to endo-*α*-*N*-acetylgalactosaminidase.[33] To confirm that the core 2 structures are located at T323, we performed MALDI-ISD MS analysis using super-DHB as a matrix. In contrast to collision-induced dissociation (CID) fragmentation in bottom-up analysis, MALDI-ISD is known to result in mainly singly charged c− and $z + 2$ ions with labile modifications remaining intact, which allows localizing O-linked glycosylation sites. MALDI-ISD MS of CHO-RBD after *N*-glycan and sialic acid removal showed N-terminal fragments (c-ions) with core 1 structure (H1N1) for the site T323 and no additional glycosylated fragments at S325 (+365.1 Da) could be detected, confirming the presence of the O-glycosylation at T323 (Figure S5A). No fragments of T323 without glycosylation were observed, indicating full-site occupancy. The analysis of HEK293-RBD comprising only core 2 structure *O*-glycans (after *N*-glycan and core 1 *O*-glycan removal) clearly showed that the core 2 structures are also located on T323 (Figure S5B). In conclusion, the combination of intact analysis of *O*-protease-treated RBDs together with MALDI-ISD allowed localizing of the *O*-glycans to the T323 with high confidence.

Assessment of RBD N-Glycosylation. We studied the two N-glycosylation sites N331 and N343 using a bottom-up glycopeptide approach combined with a step-by-step dissection of glycans at the intact level.[30] Whereas the glycopeptide data yielded the glycan composition per site, we studied the combination of these glycans at the intact level.[21]

The intact RBDs were first incubated with a mixture of sialidases and galactosidases. These enzymes removed the sialic acids and the terminal galactoses on the *N*- as well as *O*-glycans, resulting in considerably simplified deconvoluted mass spectra, as shown in Figures S6 and S7. Overall, mainly fucosylated complex type glycans were observed for both RBDs (>90.0%). This is in line with previous studies on HEK293-produced intact S protein or S1 subunit.[2,5] The dissection of the terminal galactoses also permits a direct distinction between *N*-acetyllactosamine (LacNAc) repeats and additional antenna. CHO-RBD showed a higher relative abundance of LacNAc repeats than HEK293-RBD. Additionally, CHO-RBD showed a higher antennarity, with two triantennary structures as the most abundant glycoforms, contrary to HEK293 material with di- and triantennary glycans as major signals. This was confirmed by the analysis of the glycopeptides (Figure S8, Tables S2, and S3). In general, more di- and triantennary structures were observed for HEK293-RBD (N331: 78.4% and N343: 84.5%) compared to the CHO-RBD (N331: 48.1% and N343: 72.1%). Therefore, CHO-RBD

https://doi.org/10.1021/acs.analchem.1c00893
Anal. Chem. 2021, 93, 6839−6847

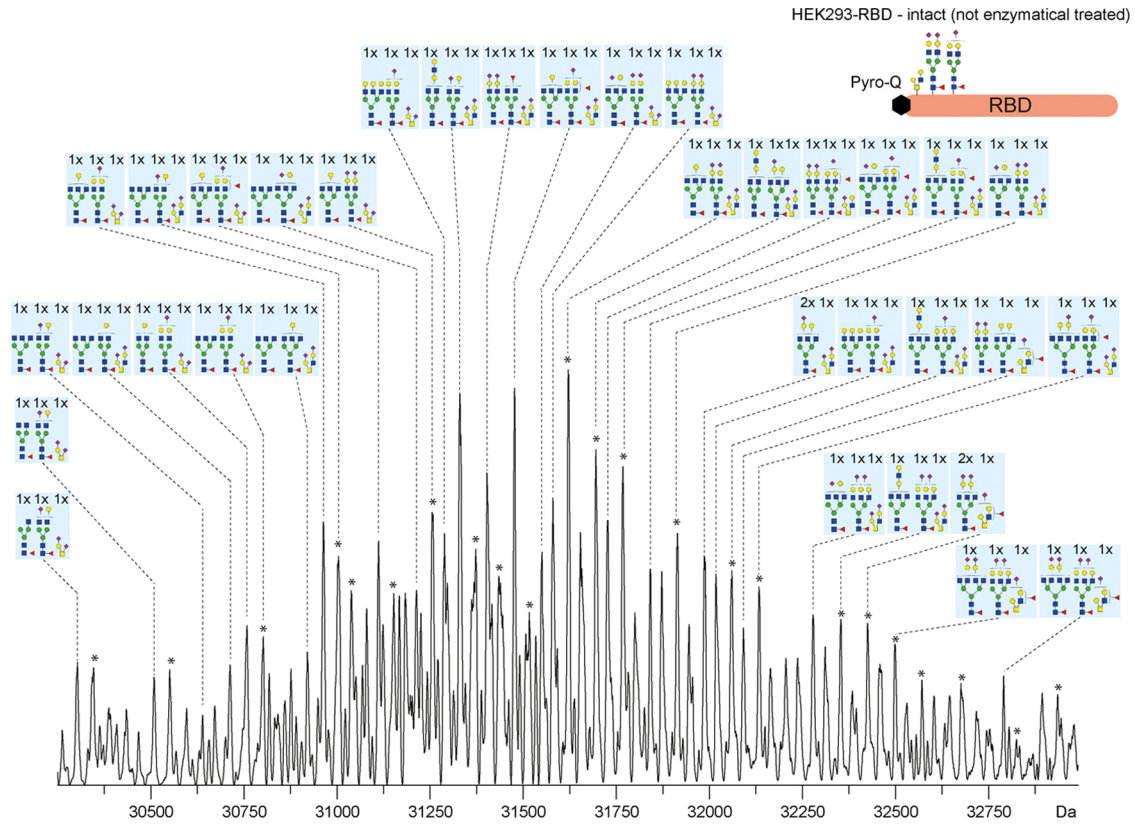

Figure 4. Deconvoluted mass spectra of the intact RBD (not enzymatically treated) produced by HEK293 cells. The assignments were based on previous enzyme treatments, mass, and glycopeptide as well as released *O*-glycan data. Peaks marked with an asterisk * are presumably the acetylated variant of RBD. Yellow square, *N*-acetylgalactosamine; yellow circle, galactose; blue square, *N*-acetylglucosamine; red triangle, fucose; and purple diamond, *N*-acetylneuraminic acid (sialic acid).

showed a larger contribution of tetraantennary structures and LacNAc repeats (N331: 42.7% and N343: 24.4%) compared to HEK293-RBD (N331: 15.7% and N343: 9.9%). Between both glycosylation sites. a difference in the number of LacNAc repeats and high antennary structures was observed with minor amounts on N343 compared to N331.

In addition, we found spurious amounts of hybrid-type glycans only at N343 and only in HEK293-RBD (0.8%), similar to previous publications.[2,5] Regarding high mannose glycans, low amounts were detected for both RBDs. In the case of HEK293-RBD, Man5 and Man6 glycans with and without phosphorylation were observed, whereas in the case of CHO-RBD, Man5 and Man6 glycans carrying an additional phosphate were detected. For HEK293-RBD, the high mannose and phosphorylated high mannose structures show combined abundances of 3.1% (N331) and 1.3% (N343) in line with the findings of Watanabe et al.[2] for the full-length S protein. For CHO-RBD, the distribution was more skewed with 7.7% (N331) and 0.9% (N343).

Besides, in the deconvoluted mass spectrum of HEK293-RBD treated with sialidase and galactosidase a pattern of signals with a mass shift of +308.1 Da was observed. A combination of one galactose and one fucose could explain this mass shift. It was shown in the literature that β-galactosidases are not able to remove the terminal galactose if antenna fucose, either linked to the galactose itself or to the *N*-acetylglucosamine, is present.[34] Therefore, we incubated HEK293-RBD either with α1-2 fucosidase and in parallel with α1-3,4 fucosidase to remove fucoses linked to the galactose and *N*-acetylglucosamine, respectively. Incubation with these fucosidases allowed the β-galactosidase to remove the terminal galactose. As shown in Figure S3, after removing the differently linked antenna fucoses, the +308.1 signals disappear completely confirming antenna fucosylation and providing information on the linkage of the antenna fucose with a predominant linkage to the *N*-acetylglucosamine. Additionally, antenna fucosylation in HEK293-RBD was confirmed by glycopeptide analysis (26.7 and 33.8% of antenna fucosylation on N331 and N343, respectively) (Figure S9, Tables S2, and S3). No antenna fucosylation was found for CHO-RBD with any of the approaches.

The analysis of the intact RBDs without any previous enzymatic treatment resulted in a very complex mass spectrum (Figures 4 and S10).

Based on the information obtained for the released *O*-glycans, glycopeptide, and enzymatically treated intact RBDs, the spectra were confidently assigned. In particular, the HEK293-RBD exhibited a large heterogeneity. In addition to the variability resulting from the acetylation and antenna fucosylation, which were not observed in CHO-RBD, also a higher degree of sialylation was observed for HEK293-RBD. This was also supported by the glycopeptide data in which CHO-RBD showed only 2.5 or 0.8% sialylated glycans, whereas HEK293-RBD contained 56.4 or 36.3% on N331 or N343, respectively (Figure S11, Tables S2, and S3). Furthermore, in CHO-RBD, only monosialylated species were observed, while in the HEK293-RBD, mono-, di-, or trisialylated species were detected. Interestingly, these high sialylation levels were not observed by Watanabe et al. who reported only 22% sialylation on N331 and 4% sialylation on

https://doi.org/10.1021/acs.analchem.1c00893
Anal. Chem. 2021, 93, 6839−6847

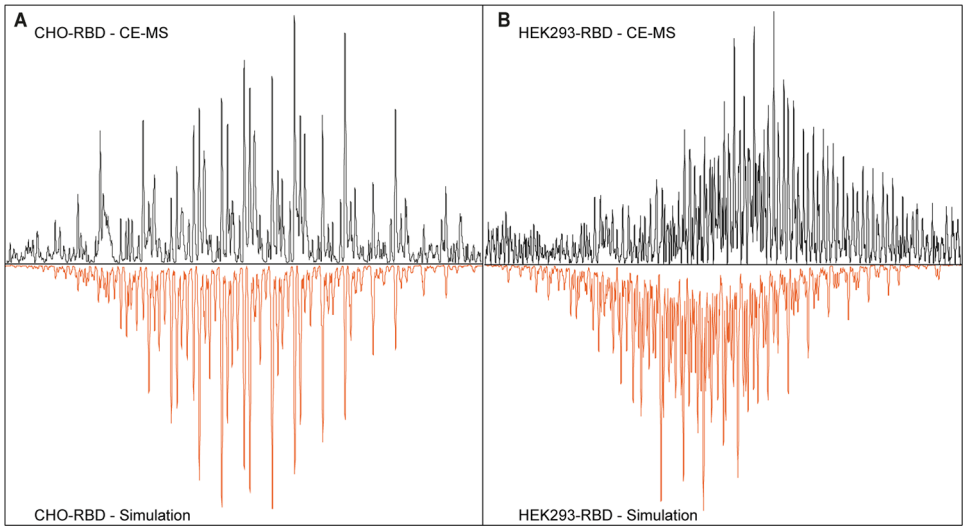

Figure 5. Deconvoluted mass spectra of the RBD intact (nonenzymatical treated) (black trace) and in silico simulated mass spectrum (vermillion trace) of RBD produced in (A) CHO cells or (B) HEK293 cells.

N343 for the full-length S protein.[2] This might be due to the different constructs with RBD expression vs the S1 subunit or S protein. A similar effect of lower sialylation on the complete S protein has also been previously reported by comparing the entire S protein expressed in HEK293 cells with the S1 subunit.[5] Whereas the S protein carried either ∼40 or 10% sialylation on N331 or N343, the S1 subunit carried 80 or 50% on N331 or N343, respectively. These findings highlight that sialylation, which influences the isoelectric point of a protein, can change with the length of the protein expressed (S, S1, or RBD) and must be taken into account.

Finally, to support our assignments, the intact mass spectra were reconstructed from the glycopeptide data as described.[21] Figure 5A shows a very strong correlation for CHO-RBD, confirming the assignments. For HEK293-RBD, the reconstructed mass spectrum showed a shift toward lower masses compared to the intact profile (Figure 5B). Proteins with higher sialylation levels often show a discrepancy between the intact and the glycopeptide-reconstructed mass spectra,[21] which could be attributable to a nonrandom combination or to a biased ionization efficiency of sialylated glycopeptides.

Functional Characterization of CHO- or HEK293-RBD. Next to the structural characterization of the RBD, a functional characterization was also performed. To assess the RBD functionality, an ACE2 receptor-binding assay and a binding assay for anti-RBD antibodies from COVID-19 patient sera were performed.

SARS-CoV-2 Antibody Binding Assay. The binding of anti-SARS-CoV-2-IgG antibodies in sera taken from 12 COVID-19 patients more than 10 weeks after the onset of the first symptoms and RBD was determined using an ELISA assay. For the assay, the intact CHO- or HEK293-RBD, as well as deglycosylated RBD samples, were used. As a negative control, a pool of 10 sera collected in 2012 was used. As expected, higher absorption values were observed for the 12 COVID-19 patient sera compared to the negative control, indicating binding of specific antibodies to the RBDs (Figure S12). Both intact RBD samples showed similar absorption values, while absorption values were slightly elevated when the deglycosylated RBDs were employed. Also, for the negative controls, the deglycosylated RBD showed elevated absorption values compared to the intact RBD. This is most probably the result of unspecific binding, which may be increased after deglycosylation. This was also reflected in the correlation of the absorption values of the patient sera. The correlation of these values gained using intact RBDs and their deglycosylated version (CHO: R^2 09681, HEK293: 0.9755) was slightly lower than the correlation obtained using intact RBD produced by CHO and HEK293 cells (R^2 0.9894) or deglycosylated CHO- vs deglycosylated HEK293-RBD (R^2 0.9905) (Figure S13).

ACE2 Receptor-Binding Assay. Using a plate-based ACE2 receptor-binding assay, dose-dependent binding of both CHO- and HEK293-RBD was observed (Figure 6A). Comparing the RBDs expressed in both production systems, similar binding properties were observed with a trend toward a lower EC_{50} value for CHO-RBD. As glycosylation has been hypothesized to have a role in the interaction with ACE2,[10,11] we additionally tested the RBDs after deglycosylation. Deglycosylation was found to reduce the binding of the RBDs, as reflected in an approximately 2 times increase of the EC_{50} values. Of note, Qianqian et al. reported that the infectivity is reduced to only 0.08% after removal of the N-glycosylation sites.[11] Our results, although they show a slight variation between the glycosylated and nonglycosylated versions, do not explain this drastic difference in infectivity. Furthermore, the presence of endoglycosidases could also have affected the biotinylation rate, resulting in the overall reduced binding values. Supporting the hypothesis of Qianqian, these glycans may be crucial for stabilizing the trimeric spike protein rather than influencing the binding affinity.[11]

Additionally, we compared the ACE2 receptor-binding affinity of both RBDs to the S1 subunit, as well as the intact S protein. The binding affinity of the ACE2 receptor to the RBDs was significantly increased compared to the S1 subunit and the S protein (Figure 6B). This might be due to the higher accessibility to ACE2 of the RBD only compared to the S1 subunit or even the S protein. As shown by Casalino et al., in the trimeric S protein, the RBD can be in an up or down conformation and, therefore, more or less accessible to the ACE2 binding.[8] Using the S protein or the S1 subunit, some parts of the RBD might not be accessible or less accessible for the ACE2 receptor, which may explain the reduced binding

https://doi.org/10.1021/acs.analchem.1c00893
Anal. Chem. 2021, 93, 6839−6847

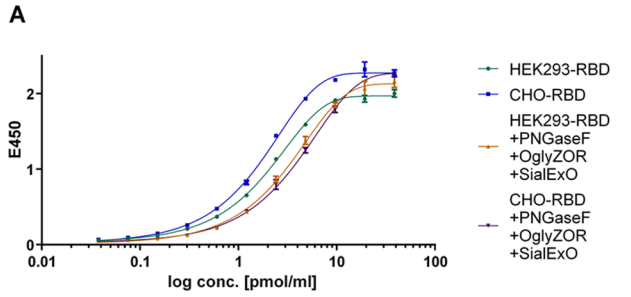

	HEK293-RBD	CHO-RBD	HEK293-RBD +PNGaseF +OglyZOR +SialExO	CHO-RBD +PNGaseF +OglyZOR +SialExO
EC_{50} [pmol/ml]	2.126	1.843	3.504	4.699

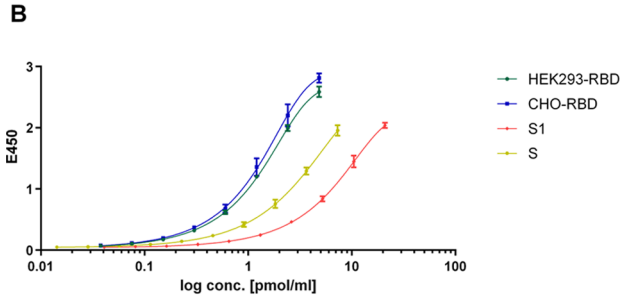

	HEK293-RBD	CHO-RBD	S1	S
EC_{50} [pmol/ml]	1.757	1.645	11.75	6.841

Figure 6. ACE2 binding assay. Dose−response curves of CHO- or HEK293-RBD binding to the ACE2 receptor. Comparison to (A) deglycosylated version of CHO- or HEK293-RBD and (B) S or S1 subunit (produced in HEK293 cells).

affinity. These results highlight the importance of the proper selection of recombinant proteins.

CONCLUSIONS

RBD proteoforms were comprehensively characterized by combining intact protein, glycopeptide, and released glycan analyses with enzymatic glycan dissection and top-down sequencing. The combination of multiple MS workflows was fundamental for assigning the intact RBD proteoforms. In particular, glycan dissection of the intact protein using sequentially different glycosidases has shown to be very powerful to annotate complex intact RBD spectra. The glycopeptide data, next to providing site-specific information, were used to simulate an in silico intact spectrum and corroborate our assignments. This approach was applied to RBD samples from both CHO and HEK293 cells. In the case of the low sialylated CHO-RBD, a very strong correlation was obtained. However, for HEK293-RBD, the simulated spectrum showed a clear shift to a lower mass associated with the loss of sialic acids or an ionization bias of the glycopeptides. This stresses the importance of assessing intact proteoforms to avoid skewing the data in any direction. The observed differences in N-glycosylation, with higher sialylation levels and antenna fucosylation for HEK293-RBD and low sialylation levels but high antennary and LacNAc repeat structures for CHO-RBD are typical for the two expression systems. For *O*-glycans, CHO-RBD showed mainly core 1 type glycans while HEK293-RBD presented a combination of core 1 and core 2 type *O*-glycans. Furthermore, using alternative approaches, such as N-terminal cleavage at the O-glycosylation site and MALDI-ISD, we localized the O-glycosylation site to T323, previously unknown. Further steps will focus on validation of the method for batch-to-batch comparison of different RBD batches and for release testing in companies producing RBD-based vaccines. Full structural characterization of the S protein instead of RBD would be challenging due to the higher molecular mass and heterogeneity (22 N-glycosylation sites). Still, some of the strategies applied in this approach, as complete deglycosylation and analysis of protein backbone or N-terminal cleavage at the O-glycosylation sites, could provide additional information to previously published studies. From a functional point of view, both RBDs showed similar binding to antibodies from COVID-19 patient sera as well as to the ACE2 receptor. The ACE2 binding was increased compared to the S protein or S1 subunit, likely due to higher accessibility. After deglycosylation, the binding of RBDs to antispike antibodies remained unaffected. For ACE2, a minor decrease in the EC_{50} values was observed, which does not fully explain the infectivity decrease with aglycosylation observed in previous studies. These findings suggest that glycosylation of the RBD plays a role in conformational stabilization rather than affecting binding affinity between ACE2 and RBD. Further studies are warranted on the influence of RBD glycosylation on S conformation, ACE2 binding, as well as virus infectivity and biology.

ASSOCIATED CONTENT

Supporting Information

The Supporting Information is available free of charge at https://pubs.acs.org/doi/10.1021/acs.analchem.1c00893.

Details on the Experimental Section; MALDI-ISD sequence coverage; deconvoluted mass spectra for the de-N-glycosylated, fucosidase-treated, and *O*-protease-treated intact RBDs; *O*-glycan site localization by MALDI-ISD; deconvoluted mass spectra for the galactosidase- and sialidase-treated RBDs; site-specific glycan-type distribution pie charts; results for the SARS-CoV-2 antibody binding assay; and relative quantification of O-released glycans and glycopeptides from RBDs (PDF)

AUTHOR INFORMATION

Corresponding Author

Elena Domínguez-Vega − *Center for Proteomics and Metabolomics, Leiden University Medical Center, 2333 ZA Leiden, The Netherlands;* orcid.org/0000-0002-6394-0783; Email: e.dominguez_vega@lumc.nl

Authors

Christoph Gstöttner − *Center for Proteomics and Metabolomics, Leiden University Medical Center, 2333 ZA Leiden, The Netherlands*

Tao Zhang − *Center for Proteomics and Metabolomics, Leiden University Medical Center, 2333 ZA Leiden, The Netherlands*

Anja Resemann − *Bruker Daltonik GmbH, 28359 Bremen, Germany*

Sophia Ruben − *InVivo BioTech Services GmbH, 16761 Hennigsdorf, Germany*

Stuart Pengelley − *Bruker Daltonik GmbH, 28359 Bremen, Germany;* orcid.org/0000-0003-2676-8096

https://doi.org/10.1021/acs.analchem.1c00893
Anal. Chem. 2021, 93, 6839−6847

Detlev Suckau − *Bruker Daltonik GmbH, 28359 Bremen, Germany;* orcid.org/0000-0002-1859-2492
Tim Welsink − *InVivo BioTech Services GmbH, 16761 Hennigsdorf, Germany*
Manfred Wuhrer − *Center for Proteomics and Metabolomics, Leiden University Medical Center, 2333 ZA Leiden, The Netherlands;* orcid.org/0000-0002-0814-4995

Complete contact information is available at: https://pubs.acs.org/10.1021/acs.analchem.1c00893

Author Contributions

C.G., T.Z., A.R., S.R., and S.P. performed measurements and processed the data. E.D.-V., M.W., T.W., and D.S. conceived the idea and designed the experiments. T.W. provided RBD samples. C.G. and E.D.-V. drafted the manuscript. C.G., T.Z., A.R., S.R., S.P., D.S., T.W., M.W., and E.D.-V. reviewed this manuscript equally.

Notes

The authors declare the following competing financial interest(s): InVivo BioTech Services is a biotechnology company producing antibodies and proteins, including SARS-CoV-2 antigens.

■ ACKNOWLEDGMENTS

The authors thank Eckhard Belau and Waltraud Evers for preparing the samples and analysis. This work was supported by the Analytics for Biologics project (Grant Agreement ID 765502) of the European Commission.

■ REFERENCES

(1) Li, H.; Liu, S.-M.; Yu, X.-H.; Tang, S.-L.; Tang, C.-K. *Int. J. Antimicrob. Agents* **2020**, *55*, No. 105951.
(2) Watanabe, Y.; Allen, J. D.; Wrapp, D.; McLellan, J. S.; Crispin, M. *Science* **2020**, *369*, 330−333.
(3) Hoffmann, M.; Kleine-Weber, H.; Schroeder, S.; Krüger, N.; Herrler, T.; Erichsen, S.; Schiergens, T. S.; Herrler, G.; Wu, N.-H.; Nitsche, A.; Müller, M. A.; Drosten, C.; Pöhlmann, S. *Cell* **2020**, *181*, 271−280.e8.
(4) Wong, S. K.; Li, W.; Moore, M. J.; Choe, H.; Farzan, M. *J. Biol. Chem.* **2004**, *279*, 3197−3201.
(5) Wang, D.; Baudys, J.; Bundy, J. L.; Solano, M.; Keppel, T.; Barr, J. R. *Anal. Chem.* **2020**, *92*, 14730−14739.
(6) Sanda, M.; Morrison, L.; Goldman, R. *Anal Chem.* **2021**, *93*, 2003−2009.
(7) Uslupehlivan, M.; Şener, E. *bioRxiv* **2020**, DOI: 10.1101/2020.03.25.007898.
(8) Casalino, L.; Gaieb, Z.; Goldsmith, J. A.; Hjorth, C. K.; Dommer, A. C.; Harbison, A. M.; Fogarty, C. A.; Barros, E. P.; Taylor, B. C.; McLellan, J. S.; Fadda, E.; Amaro, R. E. *ACS Cent. Sci.* **2020**, *6*, 1722−1734.
(9) Lan, J.; Ge, J.; Yu, J.; Shan, S.; Zhou, H.; Fan, S.; Zhang, Q.; Shi, X.; Wang, Q.; Zhang, L.; Wang, X. *Nature* **2020**, *581*, 215−220.
(10) Mehdipour, A. R.; Hummer, G. *bioRxiv* **2020**, DOI: 10.1101/2020.07.09.193680.
(11) Li, Q.; Wu, J.; Nie, J.; Zhang, L.; Hao, H.; Liu, S.; Zhao, C.; Zhang, Q.; Liu, H.; Nie, L.; Qin, H.; Wang, M.; Lu, Q.; Li, X.; Sun, Q.; Liu, J.; Zhang, L.; Li, X.; Huang, W.; Wang, Y. *Cell* **2020**, *182*, 1284−1294.e9.
(12) Premkumar, L.; Segovia-Chumbez, B.; Jadi, R.; Martinez, D. R.; Raut, R.; Markmann, A. J.; Cornaby, C.; Bartelt, L.; Weiss, S.; Park, Y.; Edwards, C. E.; Weimer, E.; Scherer, E. M.; Rouphael, N.; Edupuganti, S.; Weiskopf, D.; Tse, L. V.; Hou, Y. J.; Margolis, D.; Sette, A.; Collins, M. H.; Schmitz, J.; Baric, R. S.; de Silva, A. M. *Sci. Immunol.* **2020**, *5*, No. eabc8413.
(13) Pinto, D.; Park, Y.-J.; Beltramello, M.; Walls, A. C.; Tortorici, M. A.; Bianchi, S.; Jaconi, S.; Culap, K.; Zatta, F.; De Marco, A.; Peter, A.; Guarino, B.; Spreafico, R.; Cameroni, E.; Case, J. B.; Chen, R. E.; Havenar-Daughton, C.; Snell, G.; Telenti, A.; Virgin, H. W.; Lanzavecchia, A.; Diamond, M. S.; Fink, K.; Veesler, D.; Corti, D. *Nature* **2020**, *583*, 290−295.
(14) Zhou, D.; Tian, X.; Qi, R.; Peng, C.; Zhang, W. *Glycobiology* **2020**, *31*, 69−80.
(15) Muhuri, M.; Gao, G. *Signal Transduction Targeted Ther.* **2020**, *5*, No. 222.
(16) He, Y.; Zhou, Y.; Wu, H.; Luo, B.; Chen, J.; Li, W.; Jiang, S. *J. Immunol.* **2004**, *173*, 4050−4057.
(17) Lenza, M. P.; Oyenarte, I.; Diercks, T.; Quintana, J. I.; Gimeno, A.; Coelho, H.; Diniz, A.; Peccati, F.; Delgado, S.; Bosch, A.; Valle, M.; Millet, O.; Abrescia, N. G. A.; Palazón, A.; Marcelo, F.; Jiménez-Osés, G.; Jiménez-Barbero, J.; Ardá, A.; Ereño-Orbea, J. *Angew. Chem., Int. Ed.* **2020**, *59*, 23763−23771.
(18) Resemann, A.; Jabs, W.; Wiechmann, A.; Wagner, E.; Colas, O.; Evers, W.; Belau, E.; Vorwerg, L.; Evans, C.; Beck, A.; Suckau, D. *mAbs* **2016**, *8*, 318−330.
(19) Gstöttner, C.; Reusch, D.; Haberger, M.; Dragan, I.; Van Veelen, P.; Kilgour, D. P. A.; Tsybin, Y. O.; van der Burgt, Y. E. M.; Wuhrer, M.; Nicolardi, S. *mAbs* **2020**, *12*, No. 1682403.
(20) Santos, M. R.; Ratnayake, C. K.; Fonslow, B.; Guttman, A. *A Covalent, Cationic Polymer Coating Method for the CESI-MS Analysis of Intact Proteins and Polypeptides*, SCIEX Separations, Brea, CA, 2015.
(21) Yang, Y.; Liu, F.; Franc, V.; Halim, L. A.; Schellekens, H.; Heck, A. J. R. *Nat. Commun.* **2016**, *7*, No. 13397.
(22) Hinneburg, H.; Stavenhagen, K.; Schweiger-Hufnagel, U.; Pengelley, S.; Jabs, W.; Seeberger, P. H.; Silva, D. V.; Wuhrer, M.; Kolarich, D. *J. Am. Soc. Mass Spectrom.* **2016**, *27*, 507−519.
(23) Zhang, T.; Madunić, K.; Holst, S.; Zhang, J.; Jin, C.; ten Dijke, P.; Karlsson, N. G.; Stavenhagen, K.; Wuhrer, M. *Mol. Omics* **2020**, *16*, 355−363.
(24) Madunić, K.; Zhang, T.; Mayboroda, O. A.; Holst, S.; Stavenhagen, K.; Jin, C.; Karlsson, N. G.; Lageveen-Kammeijer, G. S. M.; Wuhrer, M. *Cell. Mol. Life Sci.* **2021**, *78*, 337−350.
(25) Karlsson, N. G.; Wilson, N. L.; Wirth, H. J.; Dawes, P.; Joshi, H.; Packer, N. H. *Rapid Commun. Mass Spectrom.* **2004**, *18*, 2282−2292.
(26) Karlsson, N. G.; Schulz, B. L.; Packer, N. H. *J. Am. Soc. Mass Spectrom.* **2004**, *15*, 659−672.
(27) Anugraham, M.; Everest-Dass, A. V.; Jacob, F.; Packer, N. H. *Rapid Commun. Mass Spectrom.* **2015**, *29*, 545−561.
(28) Ceroni, A.; Maass, K.; Geyer, H.; Geyer, R.; Dell, A.; Haslam, S. M. *J. Proteome Res.* **2008**, *7*, 1650−1659.
(29) Cooper, C. A.; Gasteiger, E.; Packer, N. H. *Proteomics* **2001**, *1*, 340−349.
(30) Wohlschlager, T.; Scheffler, K.; Forstenlehner, I. C.; Skala, W.; Senn, S.; Damoc, E.; Holzmann, J.; Huber, C. G. *Nat. Commun.* **2018**, *9*, No. 1713.
(31) Hati, S.; Bhattacharyya, S. *ACS Omega* **2020**, *5*, 16292−16298.
(32) Gstöttner, C.; Nicolardi, S.; Haberger, M.; Reusch, D.; Wuhrer, M.; Domínguez-Vega, E. *Anal. Chim. Acta* **2020**, *1134*, 18−27.
(33) Trastoy, B.; Naegeli, A.; Anso, I.; Sjögren, J.; Guerin, M. E. *Nat. Commun.* **2020**, *11*, No. 4844.
(34) Guile, G. R.; Harvey, D. J.; O'Donnell, N.; Powell, A. K.; Hunter, A. P.; Zamze, S.; Fernandes, D. L.; Dwek, R. A.; Wing, D. R. *Eur. J. Biochem.* **1998**, *258*, 623−656.